Spatial and Temporal Resolution of Shear in an Orbiting Petri Dish

Jonathan Michael D. Thomas and Amlan Chakraborty
Dept. of Chemical Engineering, University of Louisville, Louisville, KY 40292

M. Keith Sharp
Dept. of Mechanical Engineering, University of Louisville, Louisville, KY 40292

R. Eric Berson
Dept. of Chemical Engineering, University of Louisville, Louisville, KY 40292

DOI 10.1002/btpr.507
Published online February 7, 2011 in Wiley Online Library (wileyonlinelibrary.com).

It is well documented that physiological and morphological properties of anchored cells are influenced by fluid shear stress. Common orbital shakers provide a means of simultaneously applying shear stress to cells for tens to hundreds of cases by loading the shaker with multiple dishes. However, the complex flow in orbiting dishes is amenable to analytical solution for resolving shear created by the fluid motion only for simplified conditions. The only existing quantification of shear in this flow is an equation that estimates a constant scalar value of shear for the entire surface of the dish. In practice, wall shear stress (WSS) will be oscillatory rather than steady due to the travelling waveform and will vary across the surface of the dish at any instant in time. This article presents a computational model that provides complete spatial and temporal resolution of WSS over the bottom surface of a dish throughout the orbital cycle. The model is reasonably well validated by the analytical solution, with resultant WSS magnitudes that are within 0.99 ± 0.42 dyne/cm^2. The model results were compared to tangential WSS magnitudes obtained using one-dimensional optical velocimetry at discreet locations on the bottom of an orbiting dish. The experimental minimum and maximum WSS at 1 mm from the center of the dish were 6 and 7 dyne/cm^2, respectively, whereas WSS generated from the computational model ranged from 0.5 to 8.5 dyne/cm^2. The experimental minimum and maximum WSS at 12 mm from the center of the dish were 6 and 16 dyne/cm^2, respectively, whereas WSS generated from the computational model ranged from 0.5 to 14 dyne/cm^2. Discrepancies between the experimental and computational data may be attributed to a sparse sampling rate for the experimental probe, a sharp gradient at the sample area which could cause the unidirectional probe to be inaccurate if its location were not precise, and too few particles to track and a scattering of the signal by the free surface when the liquid is shallow. © 2011 American Institute of Chemical Engineers *Biotechnol. Prog.,* 27: 460–465, 2011
Keywords: computational fluid dynamics, shear stress, orbital shaker, cell cultures, petri dish

Introduction

The effects of hemodynamic forces on cellular responses have been studied for more than thirty years, yet much remains to be learned about the mechanisms linking cause and effect. Wall shear stress (WSS) is widely accepted as a primary influence affecting characteristics of anchored cells subjected to fluid flow. Endothelial cells, which line the interior walls of arteries and veins, experience shear exerted by the flow of blood, causing them to become aligned and elongated with the direction of flow and to undergo other physiological and biochemical changes (Davies et al., 1986; DePaola et al., 1992; Dewey et al., 1981; Fry, 1968; Kraiss et al., 2000; Kraiss et al., 2003; Levesque and Nerem, 1985; Satcher et al., 1992). The realization of the relationship between hemodynamic forces on the endothelium and the origins of atherosclerosis and vascular pathology, in general, has led to considerable attention focusing on the effects of these forces on cellular responses (Giddens et al., 1993; Glagov et al., 1988; Malek et al., 1999; Nerem and Levesque, 1983; Repin et al., 1984; Stehbens, 1982). Detailed, accurate information about the fluid forces acting on cells must be known to quantify the relationship between shear stresses and endothelial responses.

Several studies have been conducted in vitro using experimental apparatus that can provide accurately quantifiable shear stress over a cultured layer of endothelial cells. One type involves inducing a rotating flow field over a stationary layer of cells. In this arrangement, either a flat plate or a cone rotates over a fixed surface where the layer of cells is

J. M. D. Thomas and A. Chakraborty contributed equally to this work.

Correspondence concerning this article should be addressed to R. Eric Berson at eric.berson@louisville.edu.

anchored. An easily calculated wall shear stress is produced since the rotation rate of the upper plate or cone is known as is the height of the gap between the rotating and stationary surfaces. Another type involves flow in a chamber between two parallel plates, usually where the width and length of the plates are much larger than the gap between the plates. Again, wall shear stress is easily calculated based on the known flow rate and known gap height between the two plates.

These flow devices provide an accurate means of delivering predetermined shear stresses to a layer of cultured cells but are limited in that while steady flow is easily provided, creating oscillatory flow more complex and expensive. Perhaps more importantly, experiments must be performed consecutively rather than simultaneously unless multiple flow chamber and pumping systems are used, particularly if metabolic and other chemical signals are to remain isolated within each cell culture. Another prevalent apparatus for providing fluid motion to cultured cells is the orbital shaker platform (Asada et al., 2005; Dardik et al., 2005; Haga et al., 2003; Kraiss et al., 2000; Kraiss et al., 2003; Ley et al., 1989; Pearce et al., 1996; Yun et al., 2002). Orbital shakers allow simultaneous cell culture experiments and are widely used throughout the cell culture industry because of their simplicity. More importantly, orbital shakers provide oscillatory flow, somewhat like the pulsing fluid movement in the human vasculature system. The movement of fluid in a dish that derives its motion from an orbiting shaker platform will be oscillatory in nature with a wave whose peak rotates around the dish at an angular velocity corresponding to the orbital velocity of the dish.

Despite the prevalence and simplicity of usage, few have attempted to employ the orbiting shaker apparatus as a means for correlating shear stresses to cellular responses due to the difficulty in accurately calculating wall shear stresses exerted by the fluid. Those that have attempted to correlate shear stress in a shaker apparatus to cellular responses have used simplified means for estimating the magnitude of the shear. Ley et al. (1989) reported shear stress as a simplified constant value at the bottom of an orbiting dish as:

$$\tau_\omega = R \cdot \sqrt{\rho \cdot \mu \cdot (2 \cdot \pi \cdot f)^3} \qquad (1)$$

where R is the orbital radius, ρ is the fluid density, μ is the fluid viscosity, and f is the frequency of orbit. While the authors did not provide a derivation or reference for the origin of Eq. 1, it can be shown to be the extension of Stokes second problem for uniaxial oscillatory motion of an infinite plate beneath a fluid layer of large height to orbital motion of the plate. The equation has been widely used for estimating shear values in orbiting dishes (Dardik et al., 2005; Haga et al., 2003; Kraiss et al., 2000; Kraiss et al., 2003).

It is obvious that the Stokes second problem solution for WSS in an orbiting dish is inadequate for flow that is influenced by the free surface and/or by the walls of the dish. In such flows, anchored cells experience not a steady, constant value over the entire bottom surface of the dish, but an oscillating stress that also varies with radial position due to the "sloshing" motion of the wave that travels around the dish.

In this article, computational fluid dynamics (CFD) is employed to simulate the motion of fluid in an orbiting dish. Using FLUENT, a commercial CFD solver, a model was created that provides complete spatial and temporal resolution of WSS over the bottom surface of the dish. The results are compared with experimentally determined shear data and to the Stokes second problem analytical solution.

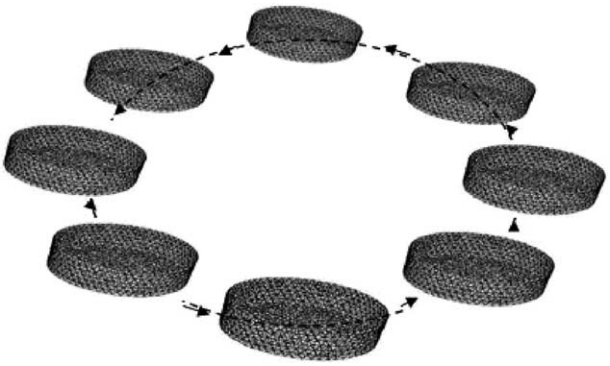

Figure 1. Model of orbital motion of dish.

Modeling and Computation

Dish dimensions, fluid properties, and orbital radius of the shaker were all defined equal to the same experimental parameters used by Dardik et al. (2005) since their work represents the limited experimental data that is currently available in the literature. A 3-D cylinder with a height of 20 mm and a radius of 17.5 mm was created in the preprocessor, GAMBIT, and then a mesh with 305,200 hexahedral computational cells was applied to the volume. This computational cell count was determined based on an optimization routine reported in Berson et al. (2008) in which the computational cell count was increased until a negligible difference in WSS magnitude and pattern was noticed after further increases in the cell count. The liquid in the dish was assigned a density of 997.3 kg m^{-3} and a viscosity of 0.00101 kg m^{-1} s^{-1}. The air above the liquid had a density of 1.225 kg m^{-3} and a viscosity of 1.7894×10^{-5} m^{-1} s^{-1}. The initial height of liquid in the dish was 2 mm.

While the fluid motion is periodic and separable, a convenient and practical approach was adopted in developing the model as an unsteady laminar flow problem in FLUENT 6.2. Defining the motion required a dynamic grid that moved through space. The orbital motion of the cylinder was defined in a user defined function (UDF) where orbital radius, orbital speed, and center of orbit were assigned; the UDF was then linked to the FLUENT solver to generate the motion. In the UDF, the orbital radius was set to 9.5 mm and the orbital speed was varied for each case. The movement of fluid due to orbital motion represents a free surface flow at the liquid-air interface. The liquid-air interface was established by the volume of fluid (VOF) model. In the VOF model, both phases across an interface share a combined set of momentum equations and the volume fraction of each fluid in each cell can be tracked throughout the grid. Surface tension was neglected. Figure 1 illustrates the orbit of the cylindrical mesh.

WSS was calculated for six cases covering the following orbital speeds: 60, 90, 120, 150, 180, and 210 rpm. Time step size was set as 0.001 sec, and the maximum number of time steps for each case was set so that the dish orbits at least 3.4 times, an amount previously determined to achieve oscillatory steady state in most cases (Berson et al., 2008). Because fluid motion at any radial position in the dish is purely periodic, convergence can be evaluated by tracking WSS values at tangential locations fixed relative to the orbital position of the dish. Convergence was defined as a

Figure 2. Resultant WSS magnitude (dyne/cm^2) and free surface contours at 120 rpm.

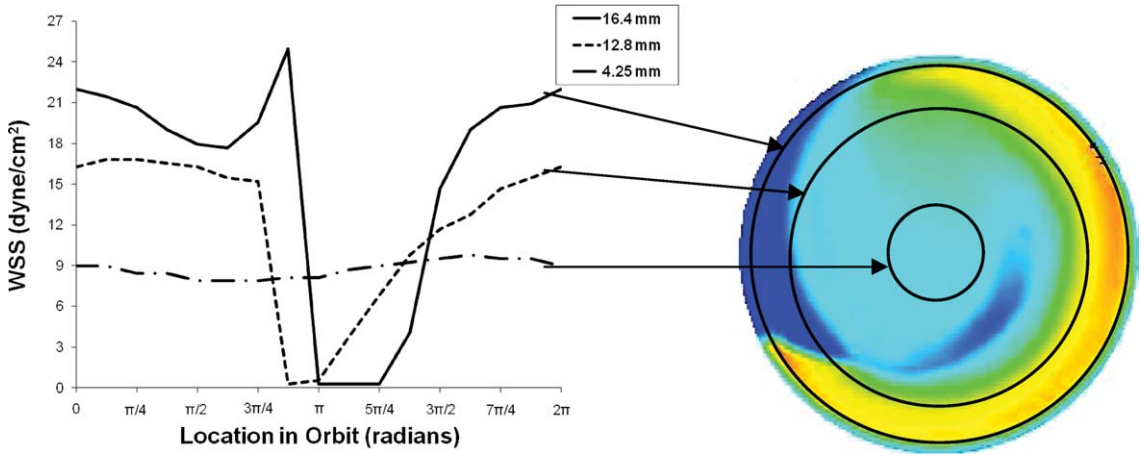

Figure 3. Resultant WSS magnitude for different radii at 210 rpm throughout one orbit (2π radians).

variance of less than ± 0.02 dyne/cm^2 between time steps, and was evaluated at the radial positions corresponding to the region of maximum WSS. The exact location of the maximum WSS region varies from case to case.

Results and Discussion

Sample simulation result

The free surface contour at a snapshot in time and the corresponding WSS contour for the 120 rpm case are shown in Figure 2 as an example of the features provided by this computational model. Whereas the widely used Eq. 1 provides a single shear value for the entire surface, the simulation exhibits significant variation of WSS over the bottom surface of the dish.

The periodicity of the flow dictates that the oscillatory steady state solution comprises a time-independent WSS contour that rotates at the speed of the orbiting motion of the dish. In this example, shear stress magnitudes are small towards the center of the dish. There is a crescent shaped region near the edge of the dish where higher shear develops. This region of maximum WSS occurs under the shallow fluid ahead of the leading edge of the wave. This phenomenon is explained by Newton's law of viscosity:

$$\tau_{zx} = -\mu\left(\frac{dv_x}{dz}\right) \tag{2}$$

where: τ_{zx} = Shear stress, μ = Viscosity of fluid, v_x = Velocity in x direction, x and z = Horizontal and vertical coordinates, respectively.

From Eq. 2, the point of highest WSS would be expected at the point with the largest velocity gradient across the fluid height. The velocity difference between the fluid surface and bottom surface, in this case, is greatest near the peak of the wave. The lowest fluid height occurs at the leading edge of the wave. The region of highest WSS appears in between these two locations (small reddish area in Figure 2) but closer to the leading edge of the wave. Several factors can influence the shape of the leading edge of the wave and the location of the maximum WSS including orbital velocity, dish diameter, fluid height, radius of orbit, density, viscosity, and gravity.

WSS as a function of radius and orbital time

Oscillating resultant WSS magnitudes on the bottom of the cylinder are shown in Figure 3 for the 210 rpm case at radial locations of 16.4 mm, 12.8 mm, and 4.25 mm from the center of the dish for one complete orbit. Near the center of the dish (inside the inner circle in the WSS contour to the right of the plot), WSS magnitudes were relatively constant throughout a complete orbit. The amplitude of oscillation increased with increasing radius, reaching a peak in amplitude, as well as magnitude, near the side wall. Finally, in a narrow band very close to the side wall (in the outer annular region in WSS contour), WSS decreased in response to the viscous layer on the side wall.

The overall nonuniformity of WSS across the dish found in these simulations correlates with differences previously observed in cellular responses based on location in the dish. For example, Dardik et al. (2005) measured increased cell proliferation and apoptosis rates, increased intercellular

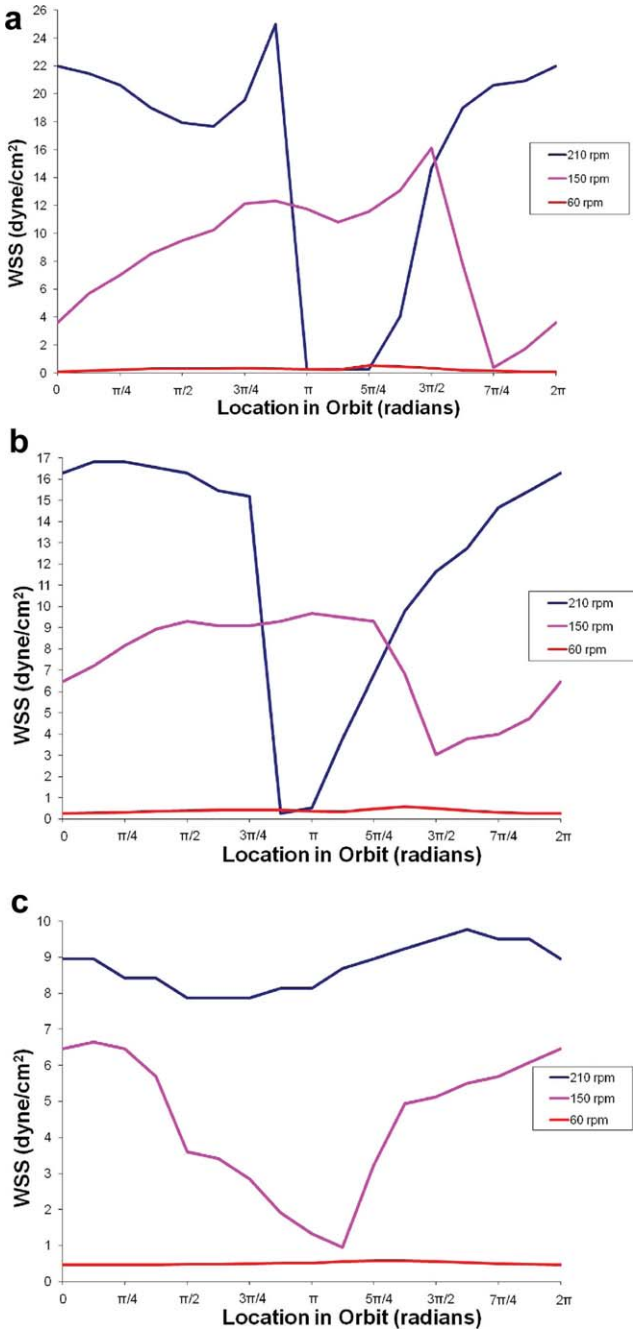

Figure 4. Resultant WSS magnitude as a function of radius and orbital velocity at radial locations of 16.4 mm (a), 12.8 mm (b), and 4.25 mm (c) throughout one orbit.

molecule adhesion expression, reduced Akt phosphorylation, and reduced E-selectin down-regulation for endothelial cells seeded in the center compared to endothelial cells seeded in the periphery of a dish. Levesque and Nerem (1985) observed rounded cells in the center of the dish (where WSS is low) and elongated cells near the edge of the dish (where WSS is high).

WSS as a function of orbital velocity

Oscillating resultant WSS magnitudes are presented for low, medium, and high orbital velocities (60, 150, and 210 rpm) at three radii on the bottom of the dish in Figures 4a–c. Values are plotted for one complete orbit. For a given radius,

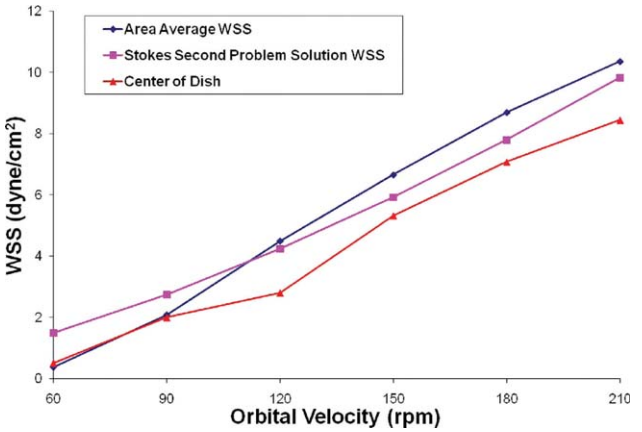

Figure 5. Comparison of area average WSS magnitude from the computational model with values from the analytical solution.

amplitudes of oscillation increased with increasing rpm, and were greater at radial locations farther from the center of the dish. At 60 rpm, WSS was nearly constant at about 0.4 dyne/cm^2 at all three radii. At 150 rpm, the peak WSS was ~6.5 dyne/cm^2 at 4.25 mm, ~9.5 dyne/cm^2 at 12.8 mm, and ~16 dyne/cm^2 at 16.4 mm. At 210 rpm, the peak WSS was ~9.5 dyne/cm^2 at 4.25 mm, ~17 dyne/cm^2 at 12.8 cm, and ~25 dyne/cm^2 at 16.4 mm. Shear values approach zero at larger radii for the 210 rpm case. While the dish does not have a dry area, the free surface becomes substantially thin at these locations, which occur under the trailing edge of the wave where velocities are lower.

Comparison with analytical solution

The Stokes second problem solution (as quantified in Eq. 1) provides an estimate for the (constant) resultant WSS magnitude for regions of the flow that are not influenced by the sides of the dish. To best match the conditions for which this analytical solution is valid, the WSS magnitudes at the center of the dish, where wall effects are least prevalent, were selected from the computational model and compared with the analytical solution (Figure 5). The area averaged WSS magnitudes from the computational model were also compared with the analytical solution. WSS values obtained using Eq. 1 followed a similar trend to the computational center WSS magnitudes throughout the range but were 0.99 $\pm$ 0.42 dyne/cm^2 higher. At 60 and 90 rpm, the center WSS magnitudes matched the area average WSS values. At 120 and higher, wall effects cause the area average WSS magnitudes to be greater than the center WSS values. The area average WSS magnitudes were also slightly higher than values from the Stokes second problem solution in this range. The area average WSS magnitudes were 0.10 $\pm$ 1.02 dyne/cm^2 higher than the Stokes second problem solution over the full range of orbital speed.

Comparison with experimental oscillatory WSS

The model was next compared to existing experimental WSS values (Dardik et al., 2005) collected using a one-dimensional optical Doppler velocimetry probe, in this case aligned to measure the tangential component. Since the probe did not distinguish between positive and negative Doppler shifts, calculated WSS values were all positive. Dardik et al. reported scatter plots of Doppler shifts (all

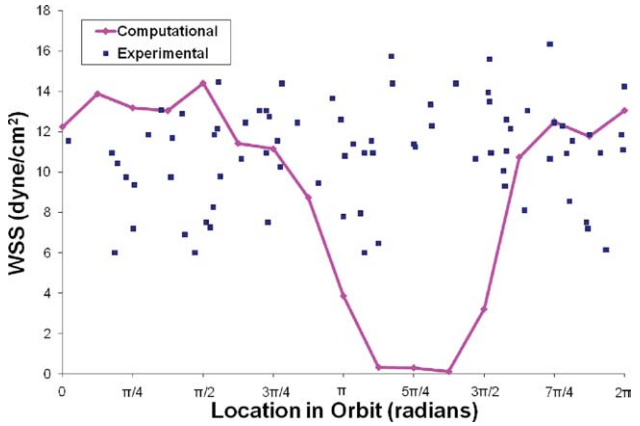

Figure 6. Comparison of computational and experimental tangential WSS magnitudes at 12 mm from center of dish and 210 rpm.

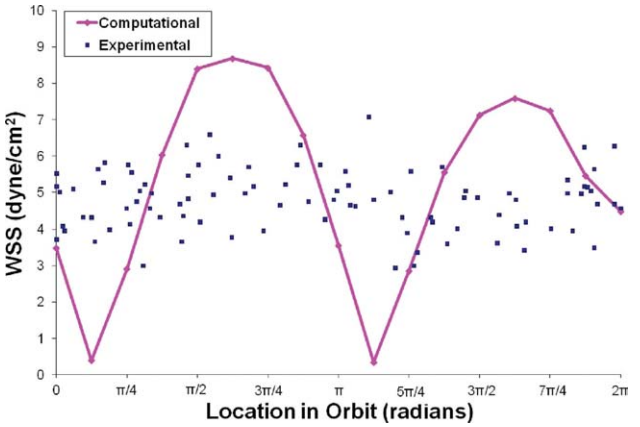

Figure 7. Comparison of computational and experimental WSS magnitudes at 1 mm from center of dish and 210 rpm.

interpreted as positive) from the ultrasonic velocity probe for a single case (210 rpm) for many orbits. (Shear stress calculated from individual Doppler shift values was not reported.) The scatter plot data converted to WSS is presented here for comparison with the computational data. The computationally determined oscillating tangential WSS magnitude for one orbit is superimposed over the WSS scatter plots in Figures 6 and 7. The scatter plots encompass 1,400 orbits for the 12 mm radial measurement position and 1,183 orbits for the 1 mm position. The sampling rates for these measurements provided one data point every 12.6 orbits at 1 mm from the center of the dish and one data point every 17.7 orbits at 12 mm from the center of the dish.

In Figure 6, the experimental minimum and maximum WSS at 12 mm from the center of the dish were 6 and 16 dyne/cm^2, respectively, whereas WSS generated from the computational model ranged from 0.5 to 14 dyne/cm^2. These match reasonably well in the upper range, but not as well in the lower range. Part of the discrepancy in the maximum value could arise since the experimental WSS values were collected in a region where the model predicts a sharp gradient in WSS in the radial direction. For instance at 210 rpm, using the simulated gradient at 12 mm, a 8% (1 mm) error in measured radial position could result in a 16 % (1.9 dyne/cm^2) error in measured WSS.

With regard to the minimum values, the sampled computational WSS magnitudes extend nearly to zero, and with greater resolution the zero crossing could be found, while the experimental WSS magnitudes plateau is much higher. There are two possible reasons for this phenomenon. First, with such a sparse sampling rate, it is possible the lowest point actually present in the experiment was not recorded during the sampling time. Second, it is also possible that the experimental probe did not pick up very low values that occur when the liquid layer was shallow over the probe. At these times, the number of TiO_2 particles over the Doppler probe would be small and scattering of the signal by the free surface would be strong enough that perhaps the signal could not be distinguished from noise and hence was not recorded by the experimental software.

In Figure 7, the measured minimum and maximum tangential WSS magnitudes at 1 mm from the center of the dish were 3 and 7 dyne/cm^2, respectively. The computational WSS magnitudes vary from 0.5 to 8.5 dyne/cm^2. The computational WSS values from 0 to $\pi/8$ and $5\pi/4$ to 2π are rectified negative values. These values do not match quite as well as those from Figure 6. There are several possible reasons for the larger differences. First, both low and high WSS measurements may have been missed due to sparse sampling. Second, an error in locating the probe measurement location, as discussed for the data in Figure 6, may have contributed to a reduction in average WSS, as well as WSS amplitude.

Conclusions

A computational model that simulates motion of fluid in a dish on an orbiting shaker apparatus has been developed. It provides a new method for determining WSS on the bottom surface of the dish with complete spatial and temporal resolution. WSS values from the computational simulation are a more useful representation of shear, since they are not limited to a constant value like current estimation methods. The computational model allows cellular response to be examined in terms of oscillating WSS values, which provides a more accurate representation of the actual shear experienced by anchored cells. The model is reasonably well validated by both an analytical solution and experimental WSS values. The model significantly enhances the usefulness of simple shaker apparatus in the study of hemodynamic effects as it is the first method to provide complete temporal and spatial resolution of WSS on endothelial and other anchored cell cultures. Complete temporal and spatial resolution can allow study of how shear effects morphology and proliferation on the entire dish, simultaneously.

Literature Cited

Asada H, Paszkowiak J, Teso D, Alvi K, Thorisson A, Frattini JC, Kudo FA, Sumpio BE, Dardik A. Sustained orbital shear stress stimulates smooth muscle cell proliferation via the extracellular signal-regulated protein kinase 1/2 pathway. *J Vasc Surg*. 2005; 42:772–780.

Berson RE, Purcell MR, Sharp MK. Computationally determined shear on cells grown in orbiting culture dishes. *Adv Exp Med Biol*. 2008;614:189–198.

Dardik A, Chen L, Frattini J, Asada H, Aziz F, Kudo FA, Sumpio BE. Differential effects of orbital and laminar shear stress on endothelial cells. *J Vasc Surg*. 2005;41:869–880.

Davies PF, Remuzzi A, Gordon EJ, Dewey CF Jr, Gimbrone MA Jr. Turbulent fluid shear stress induces vascular endothelial turnover in vitro. *Proc Natl Acad Sci*. 1986;83:2114–2117.

DePaola N, Gimbrone MA Jr, Davies PF, Dewey CF Jr. Vascular endothelium responds to fluid shear stress gradients. *Arterioscler Thromb.* 1992;12:1254–1257.

Dewey CF, Bussolari SR, Gimbrone MA, Davies PF. The dynamic response of vascular endothelial cells to fluid shear stress. *J Biomech Eng.* 1981;103:177–185.

Fry DL. Acute vascular endothelial changes associated with increased blood velocity gradients. *Circ Res.* 1968;22:165–197.

Giddens DP, Zarins CK, Glagov S. The role of fluid mechanics in the localisation and detection of atherosclerosis. *J Biomech Eng.* 1993;115:588–594.

Glagov S, Zarins CK, Giddens DP, Ku DN. Haemodynamics and atherosclerosis. Insights and perspectives gained from studies of human arteries. *Arch Pathol Lab Med.* 1988;112:1018–1031.

Haga M, Yamashita A, Paszkowiak J, Sumpio BE, Dardik A. Oscillatory shear stress increases smooth muscle cell proliferation and Akt phosphorylation. *J Vasc Surg.* 2003;37:1277–1284.

Kraiss LW, Weyrich AS, Alto NM, Dixon DA, Ennis TM, Modur V, McIntyre TM, Prescott SM, Zimmerman GA. Fluid flow activates a regulator of translation, p70/p85 S6 kinase, in human endothelial cells. *Am J Physiol.* 2000;278:H1537–H1544.

Kraiss LW, Alto NM, Dixon DA, McIntyre TM, Weyrich AS, Zimmerman GA. Fluid flow regulates E-selectin protein levels in human endothelial cells by inhibiting translation. *J Vasc Surg.* 2003;37:161–168.

Levesque MJ, Nerem RM. The elongation and orientation of cultured endothelial cells in response to shear stress. *J Biomech Eng.* 1985;107:341–347.

Ley K, Lundgren E, Berger E, Arfors K. Shear-dependent inhibition of granulocyte adhesion to cultured endothelium by dextran sulfate. *Blood.* 1989;73:1324–1330.

Malek AM, Alper SL, Izumo S. Hemodynamic shear stress and its role in atherosclerosis. *J Am Med Assoc.* 1999;282:2035–2042.

Nerem RM, Levesque MJ. Fluid dynamics as a factor in the localization of atherosclerosis. *Ann NY Acad Sci.* 1983;416:709–719.

Pearce MJ, McIntyre TM, Prescott SM, Zimmerman GA, Whatley RE. Shear stress activates cytosolic phospholipase A2 (cPLA2) and MAP kinase in human endothelial cells. *Biochem Biophys Res Commun.* 1996;218:500–504.

Repin VS, Dolgov VV, Zaikina OE, Novikov ID, Antonov AS, Nikolaeva NA, Smirnov VN. Heterogeneity of endothelium in human aorta. A quantitative analysis by scanning electron microscopy. *Atherosclerosis.* 1984;50:35–52.

Satcher RL Jr, Bussolari SR, Gimbrone MA Jr, Dewey CF Jr. The distribution of fluid forces on model arterial endothelium using computational fluid dynamics. *J Biomech Eng.* 1992;114:309–316.

Stehbens WE. Hemodynamics and atherosclerosis. *Biorheology.* 1982;19:95–101.

Yun S, Dardik A, Haga M, Yamashita A, Yamaguchi S, Koh Y, Madri JA, Sumpio BE. Transcription factor Sp1 phosphorylation induced by shear stress inhibits membrane type 1-matrix metalloproteinase expression in endothelium. *J Biol Chem.* 2002;277:34808–34814.

Manuscript received Dec. 12, 2009, and revision received July 9, 2010.